1D Wires of 2D Layered Materials: Germanium Sulfide Nanowires as Efficient Light Emitters

Eli Sutter[1,*] and Peter Sutter[2]

[1]*Department of Mechanical and Materials Engineering, University of Nebraska-Lincoln, Lincoln, NE 68588 (USA)*
[2]*Department of Electrical and Computer Engineering, University of Nebraska-Lincoln, Lincoln, NE 68588 (USA)*

ABSTRACT

We have considered the formation of 1D nanowires from the 2D layered material GeS. Growth by a low-temperature vapor-liquid-solid process over an Au catalyst gives rise to single-crystalline nanowires with typical diameters of ~100 nm and length exceeding 10 μm that consist of a crystalline GeS core with layering along the nanowire axis, surrounded by an ultrathin, sulfur-rich GeS_x shell with larger bandgap that provides chemical and electronic passivation of the nanowires. Combined variable-temperature in-situ electron microscopy, chemical mapping, and single-nanowire cathodoluminescence spectroscopy are used to uncover key elements of the growth process, and to identify the optoelectronic properties of the GeS/GeS_x core-shell nanowires. Our results suggest that vapor-liquid-solid processes can readily be extended from conventional 3D crystals to the growth of 1D wires from 2D layered crystals, and may provide novel low-dimensional materials for electronic, optoelectronic, or energy conversion applications that benefit from the wide-ranging properties of van der Waals materials.

Keywords: GeS nanowires, VLS growth, in-situ transmission electron microscopy, cathodoluminescence, optoelectronic properties, passivation

*Corresponding author: esutter@unl.edu

1. INTRODUCTION

Semiconductor nanowires have attracted significant interest due to quantum size effects and novel properties they promise to bring to a wide range of electronic and optoelectronic devices,[1-3] chemical and biological sensors,[4] artificial photosynthesis,[5] solar energy conversion,[6-7] and photovoltaic systems.[8] The majority of semiconductor nanowires have been synthesized from three-dimensional (3D) materials such as Si, Ge, GaAs, etc. Beyond these traditional semiconductors, interesting new electronic or optoelectronic functionality may become accessible in nanowires consisting of van der Waals materials. Recently, quasi-1D chalcogenides such as $Ta_2Pd_3Se_8$ or $TaSe_3$ have been isolated by exfoliation from the bulk and first studies of their properties, semiconducting for $Ta_2Pd_3Se_8$,[9] metallic or semimetallic in the case of $TaSe_3$,[10] have been reported, so far for fibers or bundles in which larger numbers of the elementary 1D units are joined by weak van der Waals forces. While the morphology of these fibers or nanowires is dictated by the 1D structure of their building blocks, an alternative avenue toward quasi 1D van der Waals materials is to shape a 2D layered crystal into a nanowire geometry. A wire geometry may be achieved by adapting bottom-up synthesis protocols that are well-established for nanowires from 3D materials, such as vapor-liquid-solid (VLS) growth.[11] Such an approach has the added advantages of producing large numbers of wires grown in parallel, and of defining the wire diameter via the size of a growth catalyst.[12-13] Here we discuss the bottom-up synthesis of nanowires of the layered semiconductor germanium sulfide (GeS) and establish the growth mechanism, structure, stability, and optoelectronic properties of these GeS wires.

GeS is a layered material with structure analogous to that of black phosphorus and a bandgap in the visible region (1.65 – 1.8 eV).[14-18] The anisotropic crystal structure of GeS gives rise to anisotropy in the optoelectronic properties, such as polarized optical absorption,[14, 18] photoconductivity,[19] etc. One important property of GeS is its much lower toxicity and environmental impact when compared with other semiconductors, e.g., those containing heavy metals such as cadmium or lead.[20] GeS nanoparticles have demonstrated excellent cycling performance for Li-ion batteries applications.[21] GeS nanosheets and nanoribbons have emerged as important IV/VI semiconductor materials with potential in electronic and opto-electronics applications[22] for telecommunications, computing, as visible light photodetectors with high sensitivity and broad spectral response,[22-24] and as a photo-absorbers for use in solar energy conversion.[25] Recent work has shown unusual electronic properties, including multiferroic behavior with coupled ferroelectricity and ferroelasticity,[26-27] and potential for third generation photovoltaics based on shift-currents.[28] In nanosheets and nanoribbons thickness-dependent properties, i.e., absorption dominated by tightly bound excitons with remarkably large binding energy of 1 eV similar to other 2D materials are expected to give rise to new phenomena in the ultrathin limit.[29] GeS nanosheets and nanoribbons have been prepared by a variety of methods: chemical vapor transport followed by mechanical exfoliation,[22, 30] chemical vapor deposition (CVD),[23, 31] and colloidal synthesis.[16, 32-33]

GeS nanowires (NWs) have previously been prepared by vapor transport[34] as well as by liquid chemical synthesis,[35-36] but an understanding of the growth mechanism, stability, and of their properties at the level of individual nanowires has not been developed. Here we discuss the synthesis of high quality GeS NWs using a low

temperature vapor-liquid-solid (VLS) process. We establish the structure of the as-grown nanowires and use transmission electron microscopy (TEM) based methods such as chemical mapping and in-situ observations of individual NWs during annealing near the growth temperature to reconstruct key elements of the VLS process, the stability of the GeS NWs, formation and decomposition pathways, and the role and behavior of the catalyst drop at the NW tip. Finally, we use cathodoluminescence in scanning transmission electron microscopy (STEM-CL) with spatial resolution below the diffraction limit to establish the optoelectronic properties of individual GeS NWs.

2. RESULTS AND DISCUSSION

GeS nanowires were grown in a two-zone tube furnace by thermal evaporation of GeS powder using Ar-2% H_2 as a carrier gas (see Methods for details). The Si(100) substrates were covered by a thin Au film, which dewets at the growth temperature (270-300°C)[37] to generate a polydisperse array of supported Au nanoparticles.

Figure 1 shows the typical structure and morphology of individual GeS NWs grown at a temperature of 280°C. The as-grown NW forests attached to the Si(100) substrate are shown in the scanning electron microscopy (SEM) image of the Supplementary Figure S1. The NWs typically have diameters in the range between 50-120 nm and grow up to several tens of micrometers long. Figures 1 (a) – (b) show high-angle annular dark field STEM (HAADF-STEM) images of a GeS NW segment on amorphous carbon support illustrating the high aspect ratio and constant diameter of the NWs over extended distances. High-resolution TEM images of the NWs (Figure S2) show lattice fringes with a separation of 0.53 nm perpendicular to the NW axis, consistent with the spacing of (002) planes in bulk GeS.[38] Selected area electron

diffraction (Figure 1 (c)) shows that the wires are monocrystalline with their axes aligned along the [001] direction, i.e., are stacks of GeS sheets with lateral dimensions limited to the NW diameter arranged with their c-axis (the van der Waals stacking direction) along the symmetry axis of the NWs (Figure 1 (d)).
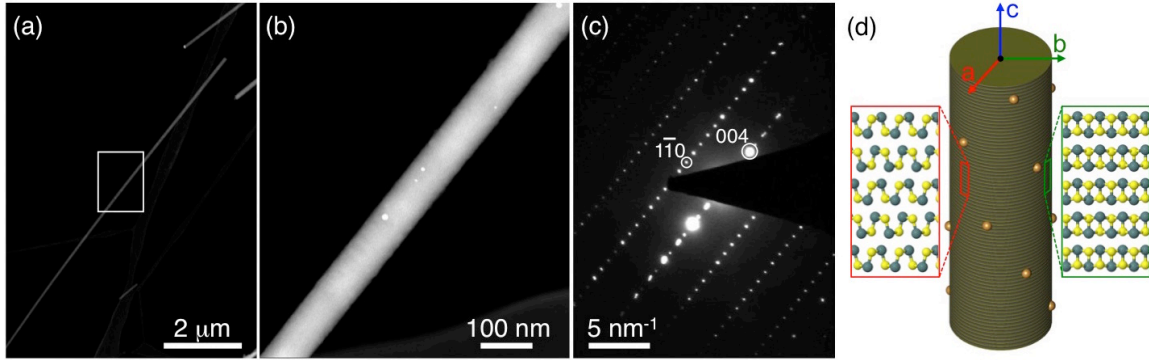

Figure 1. Morphology of GeS nanowires. **(a)** HAADF-STEM overview image of GeS NWs on amorphous carbon film (Growth temperature: 280°C). **(b)** Higher magnification HAADF-STEM image of the section of the GeS NW marked by a rectangle in (a). **(c)** Electron diffraction pattern of the GeS NW along the [110] zone axis. **(d)** Schematic representation of the layered structure of the GeS nanowires.

Figure 2 shows a HAADF-STEM image close to the tip of a GeS NW (diameter ~110 nm). The NW shows uniform contrast along its length, suggesting a homogeneous composition. Areas of brighter HAADF-STEM contrast, i.e., higher average atomic number Z, are located at the NW tip and in small nanoparticles dispersed on the NW surface. Energy dispersive x-ray spectroscopy (EDS) was used to determine the chemical composition of the NWs and of these high-Z regions. Elemental maps and spectra confirm the presence Ge and S along the NW (Figure 2 (b) – (g)), while the NW tip contains Au in addition to Ge and S (Figure 3).
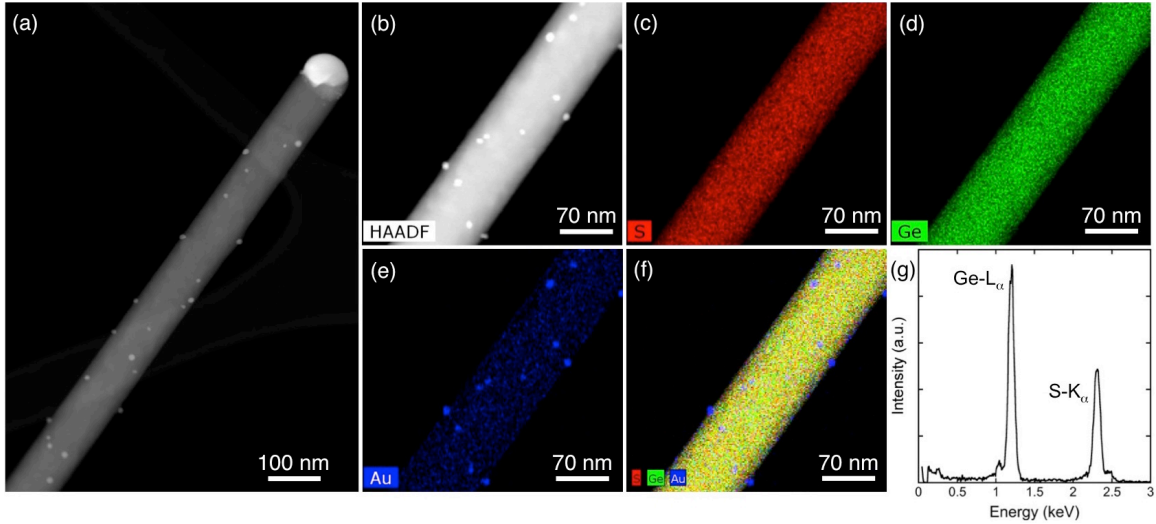
Figure 2. (a) HAADF-STEM image of a representative GeS nanowire near the Au-rich tip. **(b) –** HAADF-STEM image and **(c) – (e)** EDS chemical maps of the GeS NW showing the distribution of S (red), Ge (green), and Au (blue) **(f)** Overlaid S, Ge and Au maps. **(g)** EDS spectrum from the NW, yielding a composition of 50.2 at.% Ge and 49.8 at% S.

The chemical maps show a uniform distribution of Ge and S in the NWs (Figure 2 (c) – (f)). The quantification of spectra confirms a Ge:S atomic ratio of 1:1, corresponding to Ge monosulfide (GeS, Figure 2 (g)). Au incorporation in the NWs is below the EDS detection limit. Note that the weak signal detected in the Au EDS map across the entire NW actually originates from the tail of the S K-α EDS peak (centered at ε = 2.3 keV), which is close to the Au M peak (2.1 keV) mapped in Figure 2 (e). Intense Au signal is detected in the small nanoparticles on the NW surface, which are likely the result of Au runoff from the catalyst at the tip during cooling to room temperature, similar to VLS-grown Ge NWs.[39-40] Chemical characterization of the nanoparticle at the NW tip shows that its composition is inhomogeneous (Figure 3), comprising distinct parts that are Au-rich and Ge-rich, respectively. The Au-rich section contains substantial amounts of S as well as some Ge. The Ge-rich part of the tip, on the other hand, shows very low S and Au content.
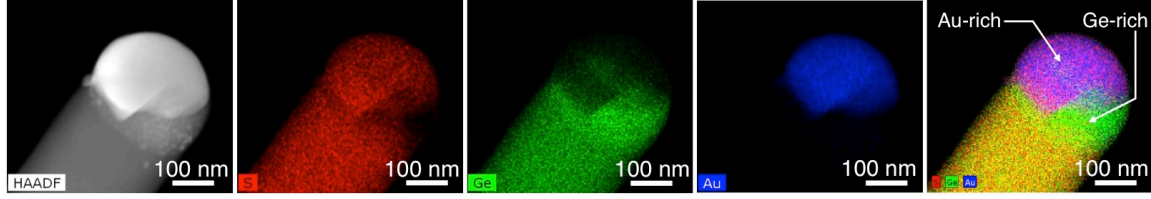
6

Figure 3. Representative HAADF-STEM image and EDS S (red), Ge (green), and Au (blue) and overlaid maps of a GeS NW tip.

The presence of telltale Au-rich catalyst particles at the tips of our GeS NWs suggests that their growth proceeds either via a vapor-liquid-solid (VLS)[34] or a vapor-solid-solid (VSS) process.[41] In both of these processes, Au nanoparticles play the role of growth seeds and transport media whose interface to the semiconductor wire represents the NW growth front. In VLS growth, the temperature is maintained above the eutectic temperature (T_E) or raised above T_E and then dropped to produce a liquid alloy drop. Surface adsorption on the drop establishes a concentration gradient of the semiconductor component in the liquid alloy, and diffusion through the drop causes a small supersaturation that drives the incorporation of new semiconductor material at the NW interface. In VSS growth the temperature is kept below the eutectic temperature and the catalyst is in the solid state, which results in much slower NW growth rates. At first glance, the low substrate temperatures (270°C) used in our experiments – lower than any eutectic temperature in the ternary Au-S-Ge alloy phase diagram – might indicate growth via a VSS process. A second possibility is that the ternary Au-S-Ge alloy might have a lower melting temperature at the nanoscale than in the bulk. Such deviations are not uncommon. For binary Au-Ge alloys, for instance, size-dependent behavior such as a lowered liquidus line and enhanced Ge solubility have been established previously using in-situ annealing experiments, and this previous work established conditions for observing melting and crystallization of the binary alloy drop.[13, 37, 42-43] Here we

performed similar in-situ experiments to obtain information on the growth of our GeS NWs, such as the underlying process (VLS or VSS), the temperature-dependent behavior (e.g., melting temperature affected by the presence of sulfur) of the Au-Ge-S tip, the elementary growth species (e.g., elemental Ge and S, or GeS molecules), and the role of the anisotropic crystal structure of GeS in growth and decomposition. Important for practical applications, the in-situ observations at variable temperature establish the thermal regime where layered GeS NWs are stable and possible new morphologies that may be accessed via controlled decomposition.

Since the catalyst particle at the NW tip holds the key to understanding the growth mechanisms, we investigated its composition and phase behavior using variable-temperature TEM. Figure 4 shows a section of a NW close to its tip during annealing from room temperature to 270°C. The NW tip initially remains solid and unchanged from its room-temperature morphology up to ~220°C. Above 230°C, parts of the tip start rearranging and at ~250°C large parts of the tip are molten (similar to Au-Ge-Sb drops at the tips of Ge NWs).[44] A small part remains solid even at 270°C, the highest temperature of our observations. Comparison with EDS maps (Figure 3) shows that it is the Ge-rich (or pure Ge) section of the tip that remains solid even at 270°C, consistent with the higher eutectic temperature for a Au-Ge alloy (361°C) or melting temperature of a Ge nanocrystal. Investigations at higher temperatures were hindered by a rapid thermal decomposition of the NWs (see below). Upon cooling to room temperature the molten tip solidifies again (Figure 4 – right, 20°C).
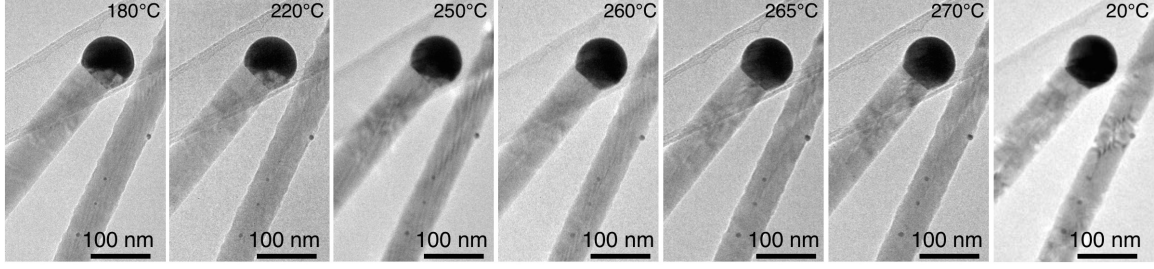
Figure 4. Sequence of TEM images showing the GeS NW close to its tip during *in-situ* annealing up to 270°C, followed by cooling to room temperature.

The Au-rich part of the NW tip contains significant amounts of both S and Ge even after the in-situ melting and re-crystallization. Previous work has shown that the melting and crystallization behavior of binary Au-Ge alloy drops depends on the Ge content: near eutectic composition all Ge is expelled upon crystallization,[11, 35] whereas this phase separation is frustrated at higher Ge content where crystallization instead produces metastable AuGe phases.[45] In the case of Au catalyzed GeS NWs, the presence of Ge and S in the Au-rich part of the tip demonstrates that not all GeS is expelled from the drop during cooling to room temperature. Strikingly, the melting temperature determined in the in-situ experiments is below ~250°C. The bulk Au-Ge-S ternary phase diagram predicts the appearance of the first liquid phase at T = 358°C, in the form of a Au-Ge eutectic in coexistence with a solid GeS phase.[46] Below 358°C the only liquid phase involves molten S coexisting with solid Au-Ge. The in-situ TEM experiments show that the Au-Ge-S tip melts at temperatures substantially below any predicted by the bulk phase diagram and is molten well below our GeS NWs growth temperatures, suggesting that the underlying growth process is VLS rather than VSS. The high growth rates (>1-2 μm/minute, as determined from the average NW length and growth duration) also suggest a VLS rather than a VSS process.

9

As mentioned above, the GeS NWs tend to decompose rapidly when heated above ~250°C. We designed in-situ annealing experiments in TEM to obtain additional information about the growth and structure from this thermal decomposition of the NWs. In principle, there are two different pathways for this process: i) Via continuous loss of S, accompanied by defect (S vacancy) formation until pure Ge is left behind, analogous to the transformation of other chalcogenides (e.g., SnS_2 to SnS[47]); or ii) by simultaneous loss of Ge and S, holding the NW composition fixed at GeS. Figure 5 follows the changes to GeS NWs during annealing (see also Supplementary Movies M1 – M3). For temperatures above 230°C, the contrast of the NWs changes with lighter areas developing and growing with time. This contrast change is associated with the loss of material from the wires. Following the thermal decomposition at temperatures between 230 and 260°C, we find that the process proceeds through identical steps and is merely slower at lower temperatures. Starting from an initially intact GeS NW (Figure 5 (a)), the onset of decomposition is clearly marked by the development of small areas of lighter contrast with rectangular or square shape developing over the surface of the NW (Figures 5 (b), (c)). These areas progressively increase in size until the entire NW is nearly completely decomposed and only a thin, empty shell is left behind. The loss of material is clearly anisotropic. It proceeds fastest in the [100] and [010] directions (i.e., by detachment from the basal plane edges) but our movies (M1 – M3) show that it also extends along the [001] direction (i.e., across the van der Waals gaps between these planes). The comparison between movies obtained at different projection of the NWs (~[100] for movie M1; ~[010] for movie M3) along with imaging of individual wires at different sample tilts (Figure S3) and measurements of the decomposition rates (Figure

10

S4) suggest an anisotropic decomposition with different detachment rates along the a- and b-axes of the GeS sheets, as well as a finite removal rate along the c-axis. The observations confirm that detachment starts at the edges (i.e., low-coordination sites) and generally proceeds into the sheet more easily than across to the neighboring sheets, which requires the nucleation of vacancies within the initially defect-free sheet. For anisotropic crystals such as GeS, different edge detachment barriers from armchair and zigzag edges may cause inhomogeneous thinning along a- and b-axes, which is indeed seen in our images.

EDS maps and spectra of annealed GeS NWs provide further insight into the decomposition process. A decreasing EDS signal intensity is consistent with the observed loss of material (Figure S5). Spectra taken at different stages of decomposition show that the NW composition is preserved, demonstrating that the thinning proceeds with a net loss of both germanium and sulfur at equal rates. This behavior is consistent with the reported high stability of GeS molecules,[48] demonstrated by the fact that in thermal evaporation of GeS powders or crystals the mass signal detected in the vapor stems solely from GeS molecules that are evaporated from the NWs as an intact unit.

The observed local thinning rather than a uniform mass loss across the entire wire surface is likely due to the presence of a thermally stable, ultrathin shell covering the NWs, which may cause local differences in the decomposition rates. This surface shell is not the result of oxidation. GeO_x would readily be reduced already at temperatures as low as 200°C,[37, 43, 49] and our EDS data do not show a significant oxygen peak (see Figure S5). Measurements of the composition of these empty shells show that they contain Ge and S, but have higher S content than the GeS NWs. Thus the decomposition of the GeS NW

leaves behind an empty GeS$_x$ "nanotube" that remains stable during annealing. Single NW luminescence measurements discussed below (Figure 6) show that this S-rich GeS$_x$ shell does not form during the annealing but is present – albeit difficult to detect by structural imaging or chemical mapping – already on the as-grown NWs and hence must be generated during the NW synthesis. Our findings differ in two key aspects from previously reported GeS$_2$ NWs:[50] (i) The present NWs are core-shell structures with a GeS core surrounded by an ultrathin sulfur-rich shell; and (ii) luminescence suggests that the shell has GeS$_x$ stoichiometry intermediate between GeS and GeS$_2$.
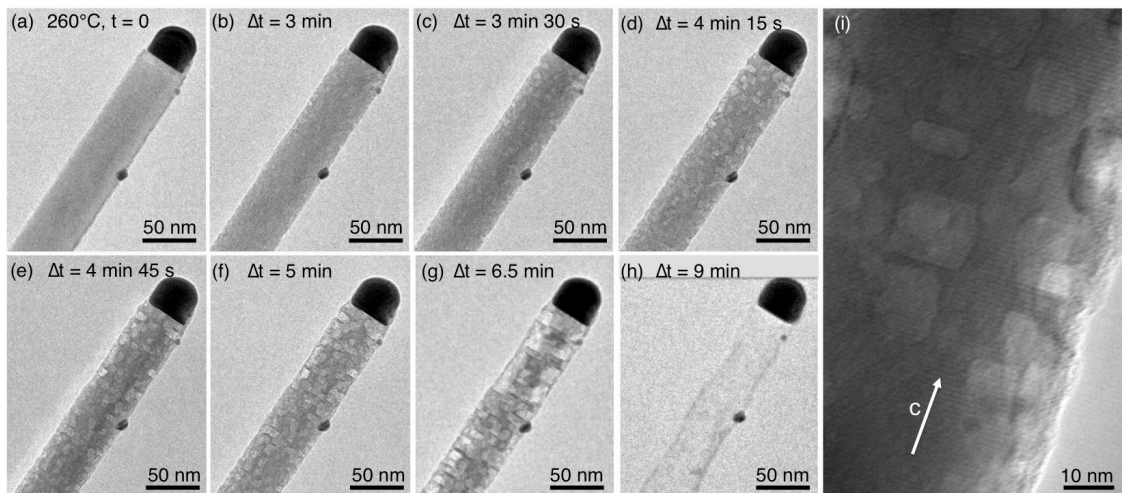

Figure 5. Sequence of TEM images of a GeS NW during annealing at 260°C over a period of 9 min. (a) – (h) In-situ TEM image image sequence showing the evolution of small rectangular-shaped thin areas in the GeS NW with time. The projection is approximately along the [100] direction of the GeS lattice. (i) High resolution TEM image at an intermediate stage of the GeS NW decomposition. The NW axis runs parallel to the c-axis of the GeS lattice.

The combined data from our structural analysis and from the annealing studies on the wires and the Au-rich catalyst particles at their tips allow us to assemble a consistent picture of the GeS NW growth process. The NWs grow by a low-temperature VLS process with a liquid, Au-rich drop as catalyst. Given that the catalyst contains both Ge and S, we conclude that during NW growth from GeS vapor the tip incorporates GeS molecules, which diffuse through the liquid drop and crystallize into a GeS NW,

analogous to the growth of other compound semiconductor NWs (GaAs, InP, etc.) from pseudo-binary alloys phases.[51-52] Predominant mass transport via stable GeS units is further confirmed by in-situ TEM experiments on the thermal decomposition of the GeS NWs. While this VLS process leads to the formation of the GeS NW core, the in-situ annealing experiments provide clear evidence for the presence of a thin GeS_x shell with higher S content. EDS maps showing a Ge-rich phase in the catalyst provide the key to understanding the formation mechanism of this shell. While most of the supplied GeS is transported through the drop intact, a small fraction appears to be dissociated into Ge and S. While the Ge accumulates in the catalyst, the S is incorporated into the NW surface during growth. Given its fixed stoichiometry, the GeS core apparently is unable to accommodate the excess sulfur, and it is thus dissipated by incorporation into an ultrathin surface shell. Assuming a shell with composition close to GeS_2, the amount of residual Ge in the tip after growth yields an estimated shell thickness of ~1 nm (see Supplement, Figure S6). Importantly, this shell provides an efficient passivation against any chemical changes in the NWs over months (Figure S7).[53]

To evaluate the optoelectronic properties of the GeS-GeS_x core-shell NWs, we performed cathodoluminescence (CL) spectroscopy in STEM. The high spatial resolution of STEM-CL enabled the acquisition of luminescence spectra and of spectrum scans across individual wires. There have been few reports of photoluminescence of GeS. Early absorption measurements give a bandgap of GeS between 1.6 and 1.8 eV.[14-18] Similar values were found more recently in diffuse reflectance measurements on GeS nanosheets.[32] GeS flakes exfoliated from bulk crystals showed a single PL peak at 1.66 eV, a decreasing PL intensity with decreasing flake thickness, and a distinct anisotropy in

the optical absorption demonstrated by rotating the polarization with respect to the crystal axes.[30] Ensembles of thick (200 nm diameter) nominally GeS NWs showed a wide PL peak centered at high energy 2.64 eV (470 nm), close to the absorption edge of GeS_2 nanoplates detected at 2.75 eV (450 nm),[35] but no emission at lower photon energies was detected. This strongly suggests that PL of these NWs was dominated by GeS_2, which was indeed detected by X-ray diffraction as well.
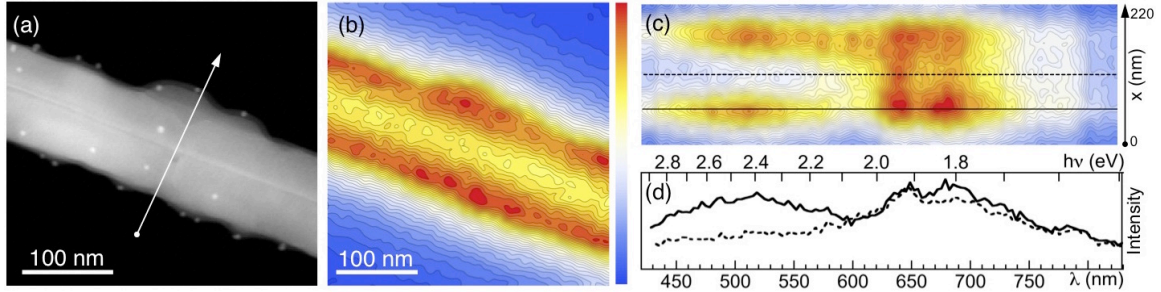

Figure 6. STEM-CL on individual as-grown and annealed GeS NWs. **(a)** STEM image of a section of an as-grown GeS NW. **(b)** Panchromatic CL map of the GeS NW shown in (a). The false color scale is given on the right. **(c)** Spectrum imaging linescan across the NW, as marked in (a). The abscissa (wavelength, λ or photon energy, hν) is the same as in (c). **(d)** Local luminescence spectra from the center (dashed) and periphery (solid) of the NW (at positions indicated in (c)).

Figure 6 shows CL maps and spectra obtained on individual as-grown GeS NWs. The wires show intense luminescence across the visible parts of the spectrum. In panchromatic CL maps, a pronounced maximum in emission intensity is observed near the surface of the NWs, which in projection is seen as two intense bands near the top and bottom edges of the wire (Figure 6 (a), (b)). Sets of CL spectra collected along a line across the NW (as shown in Figure 6 (c), (d)) can explain this intensity distribution. Two main emission peaks at ~645 and 685 nm (i.e., ~1.92 and 1.80 eV) are detected in the center of the as-grown NWs, close to peaks observed previously in unpolarized room temperature absorption spectra on bulk GeS.[54] Significant emission extends in a tail to longer wavelengths. These data are consistent with luminescence from the GeS core of

the NWs. In the near-surface region, a distinctly different characteristic is found. In addition to the two peaks also present in the NW core emission, we find an additional, broader emission peak centered at ~515 nm (i.e., 2.40 eV), which is clearly associated with the GeS_x shell. Interestingly, the emission peaks found in the GeS core appear with higher intensity near the surface. This finding suggests an enhanced radiative recombination due to electronic passivation by the ultrathin wide-bandgap GeS_x shell, which effectively reflects minority carriers toward the GeS core, i.e., away from possible non-radiative recombination centers at the NW surface. This passivation due to the wide-bandgap shell – and possibly also a reduced effect in layered materials of impurities that would give rise to deep level recombination centers in ordinary semiconductors – thus explains the absence of luminescence quenching due to surface recombination or due to trap states that might be induced by the Au particles located on the NW surface.

3. CONCLUSIONS

In summary, we have studied the formation of 1D nanowires from the 2D layered material GeS. Growth by a low-temperature vapor-liquid-solid process over an Au catalyst gives rise to single-crystalline nanowires with typical diameters of ~100 nm and length exceeding 10 μm that predominantly consist of GeS that is layered along the nanowire axis. In-situ electron microscopy of the thermal decomposition of the nanowires suggests that individual intact GeS units are thermally stable at the growth temperature, and are the predominant mobile species adsorbed on and transported through the Au-based catalyst drop during the vapor-liquid-solid growth process. The involved nanoscale pseudo-binary (Au/GeS) phase appears to have an extremely low melting point, identified here by variable-temperature in-situ microscopy to be ~250°C, which enables growth via

a liquid catalyst at temperatures substantially below those used for nanowire growth in related materials systems (e.g., Au-Ge). For nanowires consisting of layered materials, one might raise concerns about a possible detrimental role of a large number of dangling bonds at the edges of the layers, especially in the configuration found here, namely with layering perpendicular to the long axis of the wires. By combining observations of the nanowire decomposition with results from local luminescence spectroscopy, we identify an ultrathin shell, consisting of more sulfur-rich GeS_x, around the layered GeS core. This finding implies that layered VLS nanowires may be able to self-passivate dangling bonds at their surface during growth. In the present case, the morphology of the catalyst at the GeS nanowire tip – comprising a part that is highly enriched in Ge – suggests that an ultrathin passivating shell is generated during growth by incorporation of sulfur liberated by the dissociation of a small fraction of the adsorbing GeS in the catalyst drop. Our results suggest that vapor-liquid-solid processes lend themselves well to the growth of 1D wires from 2D layered crystals, and that such processes may enable the generation of novel low-dimensional materials for electronic, optoelectronic, or energy conversion applications that benefit from the wide-ranging properties of van der Waals materials.

4. MATERIALS AND METHODS

GeS NWs were synthesized using GeS powder (99.99%, Sigma Aldrich) in an experimental setup consisting of a pumped quartz tube furnace with two temperature zones. The evaporation zone containing a quartz boat with the GeS powder was heated to 450°C, while the zone containing the substrate was heated to growth temperatures of 270-350°C. Si (100) covered with 2-4 nm thick Au films deposited by sputtering at room temperature was used as substrate. Such Au films dewet at the growth temperature.[37]

During growth a H_2 (2%)/Ar carrier gas flow was maintained at 50 standard cubic centimeters per minute (sccm) at a pressure of 20 mTorr. The growth was typically performed for 10 minutes resulting in the formation of NWs with lengths of several tens of micrometers. The morphology of the NWs was investigated by transmission electron microscopy (TEM) in an FEI Technai Osiris 80-200 ChemiSTEM field emission microscope and an FEI Talos F200X equipped with a Gatan 652 high-temperature sample holder. In-situ experiments in TEM cover the temperature range between room temperature and 300°C at pressures below 10^{-7} torr. The electron irradiation intensity was kept intentionally low (< 0.1 A/cm^2) during our observations to prevent any uncontrolled electron beam induced structural changes. Cathodoluminescence (CL) measurements were performed in STEM mode (STEM-CL) using a Gatan Vulcan CL holder at room temperature and 200 kV electron energy. The incident beam current for CL measurements was typically 300-400 pA. The panchromatic CL map in figure 6 is 100×100 pixels with acquisition time of 100 ms per pixel. Spectrum line scans were acquired by rastering the electron beam in small steps across individual NWs and acquiring full CL spectra at each beam position.

5. ACKNOWLEDGEMENTS

SUPPORTING INFORMATION AVAILABLE: Supplementary Figures S1-S7: SEM of GeS nanowires on the growth substrate, TEM images and chemical maps of pristine and thermally decomposed GeS nanowires, analysis of decomposition rates, EDS spectra

of as grown and long-term air exposed GeS nanowires. Supplementary Movies M1-M3: In-situ microscopy of thermal decomposition of GeS nanowires.

REFERENCES:

1.   Lu, W.; Xiang, J.; Timko, B. P.; Wu, Y.; Lieber, C. M. One-Dimensional Hole Gas in Germanium/Silicon Nanowire Heterostructures P Natl Acad Sci USA **2005**, 102, 10046-10051.
2.   Wang, D. W.; Wang, Q.; Javey, A.; Tu, R.; Dai, H. J.; Kim, H.; McIntyre, P. C.; Krishnamohan, T.; Saraswat, K. C. Germanium Nanowire Field-Effect Transistors with Sio2 and High-Kappa Hfo2 Gate Dielectrics Appl Phys Lett **2003**, 83, 2432-2434.
3.   Zhang, L.; Tu, R.; Dai, H. J. Parallel Core-Shell Metal-Dielectric-Semiconductor Germanium Nanowires for High-Current Surround-Gate Field-Effect Transistors Nano Lett **2006**, 6, 2785-2789.
4.   Kamins, T. I.; Sharma, S.; Yasseri, A. A.; Li, Z.; Straznicky, J. Metal-Catalysed, Bridging Nanowires as Vapour Sensors and Concept for Their Use in a Sensor System Nanotechnology **2006**, 17, S291-S297.
5.   Liu, C.; Dasgupta, N. P.; Yang, P. Semiconductor Nanowires for Artificial Photosynthesis Chemistry of Materials **2014**, 26, 415-422.
6.   Liu, S.; Tang, Z.-R.; Sun, Y.; Colmenares, J. C.; Xu, Y.-J. One-Dimension-Based Spatially Ordered Architectures for Solar Energy Conversion Chemical Society Reviews **2015**, 44, 5053-5075.
7.   Su, Y.; Liu, C.; Brittman, S.; Tang, J.; Fu, A.; Kornienko, N.; Kong, Q.; Yang, P. Single-Nanowire Photoelectrochemistry Nat Nano **2016**, 11, 609-612.
8.   Brittman, S.; Gao, H.; Garnett, E. C.; Yang, P. Absorption of Light in a Single-Nanowire Silicon Solar Cell Decorated with an Octahedral Silver Nanocrystal Nano Lett **2011**, 11, 5189-5195.
9.   Xue Liu; Jinyu Liu; Liubov Yu. Antipina; Jin Hu; Chunlei Yue; Ana M. Sanchez; Pavel B. Sorokin; Zhiqiang Mao; Wei, J. Direct Fabrication of Functional Ultrathin Single-Crystal Nanowires
from Quasi-One-Dimensional Van Der Waals Crystals Nano Lett **2016**, 16, 6188-6195.
10.   Guanxiong Liu; Sergey Rumyantsev; Matthew A. Bloodgood; Tina T. Salguero; Michael Shur; Balandin, A. A. Low-Frequency Electronic Noise in Quasi-1d Tase3 Van Der Waals
Nanowires Nano Lett **2017**, 17, 377-383.
11.   Wagner, R. S.; Ellis, W. C. Vapor‐Liquid‐Solid Mechanism of Single Crystal Growth Appl Phys Lett **1964**, 4, 89-90.
12.   Dayeh, S. A.; Picraux, S. T. Direct Observation of Nanoscale Size Effects in Ge Semiconductor Nanowire Growth Nano Lett **2010**, 10, 4032-4039.
13.   Sutter, E.; Sutter, P. Phase Diagram of Nanoscale Alloy Particles Used for Vapor−Liquid−Solid Growth of Semiconductor Nanowires Nano Lett **2008**, 8, 411-414.
14.   Wiley, J. D.; Breitschwerdt, A.; Schonherr, E. Optical-Absorption Band Edge in Single-Crystal Ges Solid State Commun **1975**, 17, 355-359.
15.   Bletskan, D. I.; Polazhinets, N. V.; Gal, M. M. Photoelectric Properties of Layered Crystals of Ges Doped with Sb Inorg Mater **1989**, 25, 1375-1378.

16.   Ramasamy, P.; Kwak, D.; Lim, D.-H.; Ra, H.-S.; Lee, J.-S. Solution Synthesis of Ges and Gese Nanosheets for High-Sensitivity Photodetectors Journal of Materials Chemistry C **2016**, 4, 479-485.

17.   Yabumoto, T. Electrical and Optical Properties of Ges J Phys Soc Jpn **1958**, 13, 559-562.

18.   Gamzaev, D. O.; Kulibekov, A. M.; Suleimanov, R. A. Light-Exciton Mixing Effects in Ges Inorg Mater **1992**, 28, 1992-1994.

19.   Wiley, J. D.; Pennington, S.; Schonherr, E. Anisotropy of the Intrinsic Photoconductivity of Ges Phys Status Solidi B **1979**, 96, K43-K46.

20.   Latiff, N.; Teo, W. Z.; Sofer, Z.; Huber, S.; Fisher, A. C.; Pumera, M. Toxicity of Layered Semiconductor Chalcogenides: Beware of Interferences Rsc Adv **2015**, 5, 67485-67492.

21.   Cho, Y. J.; Im, H. S.; Myung, Y.; Kim, C. H.; Kim, H. S.; Back, S. H.; Lim, Y. R.; Jung, C. S.; Jang, D. M.; Park, J.; Cha, E. H.; Choo, S. H.; Song, M. S.; Cho, W. I. Germanium Sulfide(Ii and Iv) Nanoparticles for Enhanced Performance of Lithium Ion Batteries Chemical Communications **2013**, 49, 4661-4663.

22.   Ulaganathan, R. K.; Lu, Y.-Y.; Kuo, C.-J.; Tamalampudi, S. R.; Sankar, R.; Boopathi, K. M.; Anand, A.; Yadav, K.; Mathew, R. J.; Liu, C.-R.; Chou, F. C.; Chen, Y.-T. High Photosensitivity and Broad Spectral Response of Multi-Layered Germanium Sulfide Transistors Nanoscale **2016**, 8, 2284-2292.

23.   Lan, C.; Li, C.; Yin, Y.; Guo, H.; Wang, S. Synthesis of Single-Crystalline Ges Nanoribbons for High Sensitivity Visible-Light Photodetectors Journal of Materials Chemistry C **2015**, 3, 8074-8079.

24.   Dhanabalan, S. C.; Ponraj, J. S.; Zhang, H.; Bao, Q. L. Present Perspectives of Broadband Photodetectors Based on Nanobelts, Nanoribbons, Nanosheets and the Emerging 2d Materials Nanoscale **2016**, 8, 6410-6434.

25.   Antunez, P. D.; Buckley, J. J.; Brutchey, R. L. Tin and Germanium Monochalcogenide Iv-Vi Semiconductor Nanocrystals for Use in Solar Cells Nanoscale **2011**, 3, 2399-2411.

26.   Fei, R.; Li, W.; Li, J.; Yang, L. Giant Piezoelectricity of Monolayer Group Iv Monochalcogenides: Snse, Sns, Gese, and Ges Appl Phys Lett **2015**, 107, 173104.

27.   Wu, M.; Zeng, X. C. Intrinsic Ferroelasticity and/or Multiferroicity in Two-Dimensional Phosphorene and Phosphorene Analogues Nano Lett **2016**, 16, 3236–3241.

28.   Kushnir, K.; Wang, M.; Fitzgerald, P. D.; Koski, K. J.; Titova, L. V. Ultrafast Zero-Bias Photocurrent in Ges Nanosheets: Promise for Photovoltaics ACS Energy Letters **2017**, 2, 1429–1434.

29.   Gomes, L. C.; Trevisanutto, P. E.; Carvalho, A.; Rodin, A. S.; Castro Neto, A. H. Strongly Bound Mott-Wannier Excitons in Ges and Gese Monolayers Physical Review B **2016**, 94, 155428.

30.   Tan, D.; Lim, H. E.; Wang, F.; Mohamed, N. B.; Mouri, S.; Zhang, W.; Miyauchi, Y.; Ohfuchi, M.; Matsuda, K. Anisotropic Optical and Electronic Properties of Two-Dimensional Layered Germanium Sulfide Nano Research **2017**, 10, 546-555.

31.   Li, C.; Huang, L.; Snigdha, G. P.; Yu, Y. F.; Cao, L. Y. Role of Boundary Layer Diffusion in Vapor Deposition Growth of Chalcogenide Nanosheets: The Case of Ges Acs Nano **2012**, 6, 8868-8877.

32.   Vaughn, D. D.; Patel, R. J.; Hickner, M. A.; Schaak, R. E. Single-Crystal Colloidal Nanosheets of Ges and Gese J Am Chem Soc **2010**, 132, 15170-15172.

33.   Vaughn, D. D.; Schaak, R. E. Synthesis, Properties and Applications of Colloidal Germanium and Germanium-Based Nanomaterials Chemical Society Reviews **2013**, 42, 2861-2879.

34.   Li, C.; Yu, Y. F.; Chi, M. F.; Cao, L. Y. Epitaxial Nanosheet-Nanowire Heterostructures Nano Lett **2013**, 13, 948-953.

35.   Lai, Z.; Guo, Y.; Yang, P. Facile Synthesis, Characterization, Nanocrystal Growth and Photoluminescence Properties of Ges Nanowires Nano **2016**, 11, 1650140.

36.   Shi, L.; Dai, Y. M. Synthesis, Formation Mechanism and Photoelectric Properties of Ges Nanosheets and Nanowires J Appl Crystallogr **2014**, 47, 527-531.

37.   Sutter, E.; Ozturk, B.; Sutter, P. Selective Growth of Ge Nanowires by Low-Temperature Thermal Evaporation Nanotechnology **2008**, 19.

38.   Wiedemeier, H.; Schnering, H. G. V. Refinement of the Structures of Ges, Gese, Sns and Snse Z Kristallogr **1978**, 148, 295-303.

39.   Sutter, E.; Sutter, P. Au-Induced Encapsulation of Ge Nanowires in Protective Carbon Shells Adv Mater **2006**, 18, 2583.

40.   Kamins, T. I.; Li, X.; Williams, R. S. Growth and Structure of Chemically Vapor Deposited Ge Nanowires on Si Substrates Nano Lett **2004**, 4, 503.

41.   Chou, Y. C.; Wen, C. Y.; Reuter, M. C.; Su, D.; Stach, E. A.; Ross, F. M. Controlling the Growth of Si/Ge Nanowires and Heterojunctions Using Silver-Gold Alloy Catalysts Acs Nano **2012**, 6, 6407-6415.

42.   Sutter, E. A.; Sutter, P. W. Size-Dependent Phase Diagram of Nanoscale Alloy Drops Used in Vapor-Liquid-Solid Growth of Semiconductor Nanowires Acs Nano **2010**, 4, 4943-4947.

43.   Sutter, P. W.; Sutter, E. A. Dispensing and Surface-Induced Crystallization of Zeptolitre Liquid Metal-Alloy Drops Nat Mater **2007**, 6, 363-366.

44.   Sutter, E.; Sutter, P. Vapor-Liquid-Solid Growth and Sb Doping of Ge Nanowires from a Liquid Au-Sb-Ge Ternary Alloy Appl Phys a-Mater **2010**, 99, 217-221.

45.   Sutter, E.; Sutter, P. Formation and Stabilization of Single-Crystalline Metastable Auge Phases in Ge Nanowires Nanotechnology **2011**, 22.

46.   Moh, G. H.; Kullerud, G. Gold-Germanium-Sulfur Ternary Alloy Phase Diagram Neues Jahrbuch Fur Mineralogie-Abhandlungen **1986**, 153, 307-310.

47.   Sutter, E.; Huang, Y.; Komsa, H. P.; Ghorbani-Asl, M.; Krasheninnikov, A. V.; Sutter, P. Electron-Beam Induced Transformations of Layered Tin Dichalcogenides Nano Lett **2016**, 16, 4410-4416.

48.   Mills, K. C., *Thermodynamic Data for Inorganic Sulphides, Selenides and Tellurides.* Butterworths: London, 1974.

49.   Sutter, E.; Sutter, P. Au-Induced Encapsulation of Ge Nanowires in Protective C Shells Adv Mater **2006**, 18, 2583-+.

50.   Nath, M.; Choudhury, A.; Rao, C. N. R. Chemical Routes to Ges2 and Gese2 Nanowires Chemical Communications **2004**, 2698-2699.

51.   Panish, M. B. Ternary Condensed Phase Systems of Gallium and Arsenic with Group Ib Elements J Electrochem Soc **1967**, 114, 516-&.

52.   Duan, X.; Lieber, C. M. General Synthesis of Compound Semiconductor Nanowires Adv Mater **2000**, 12, 298-302.

53.   Chen, H.; Keiser, C.; Du, S.; Gao, H.-J.; Sutter, P.; Sutter, E. Termination of Ge Surfaces with Ultrathin Ges and Ges2 Layers Via Solid-State Sulfurization Physical Chemistry Chemical Physics **2017**, In Press, DOI 10.1039/C7CP05990F.

54.   Bletskan, D. I.; Madyar, I. I.; Mikulaninets, S. V.; Sichka, M. Y. Electrical and Photoelectric Properties of Ges Layered Crystals Grown by Different Techniques Inorg Mater **2000**, 36, 544-550.

For Table of Contents Only

TOC Graphic
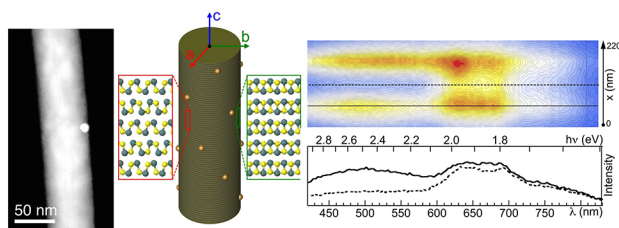
Supporting Information

1D Wires of 2D Layered Materials: Germanium Sulfide Nanowires as Efficient Light Emitters

Eli Sutter[1,*] and Peter Sutter[2]

[1]*Department of Mechanical and Materials Engineering, University of Nebraska-Lincoln, Lincoln, NE 68588 (USA)*
[2]*Department of Electrical and Computer Engineering, University of Nebraska-Lincoln, Lincoln, NE 68588 (USA)*

*Corresponding author: esutter@unl.edu

1. Supplementary Figures
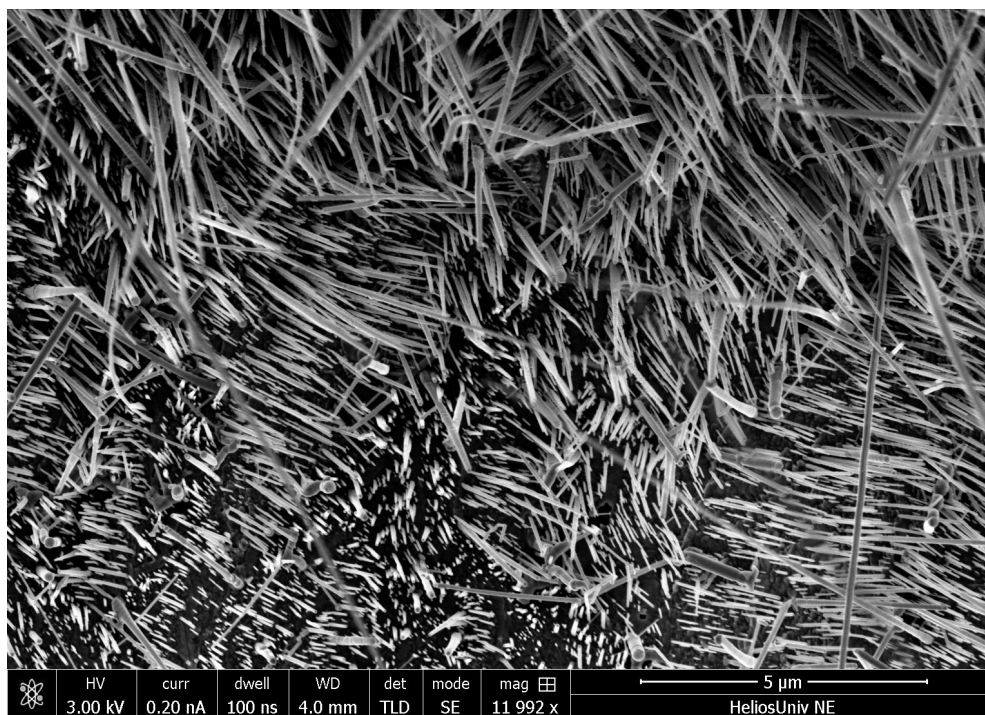
Figure S1. GeS nanowire forests on the growth substrate. SEM image of GeS nanowires grown on Si (100) substrate covered with nominally 2 nm Au film.
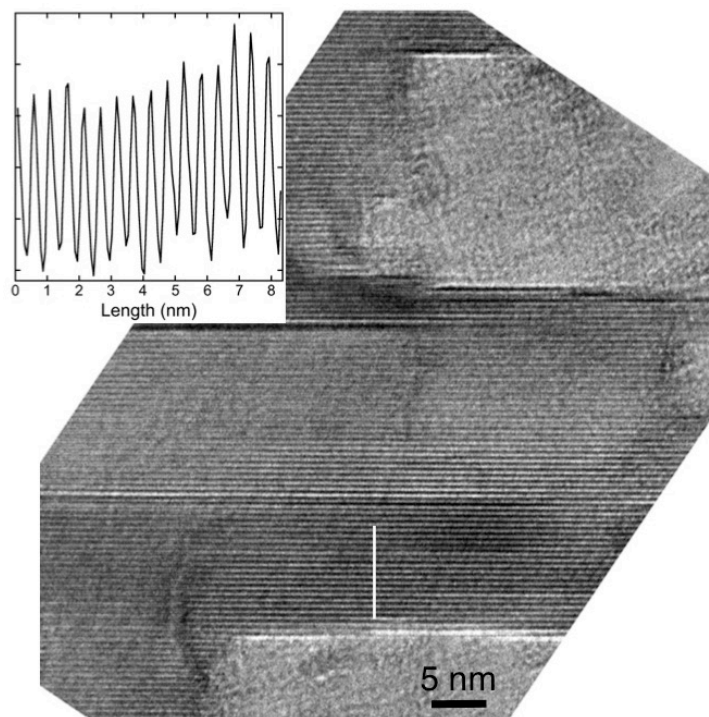
Figure S2. High-resolution TEM of a GeS nanowire. HR-TEM image showing (002) lattice fringes with a spacing of 0.53 nm. The inset shows an intensity profile along the white line marked in the image.
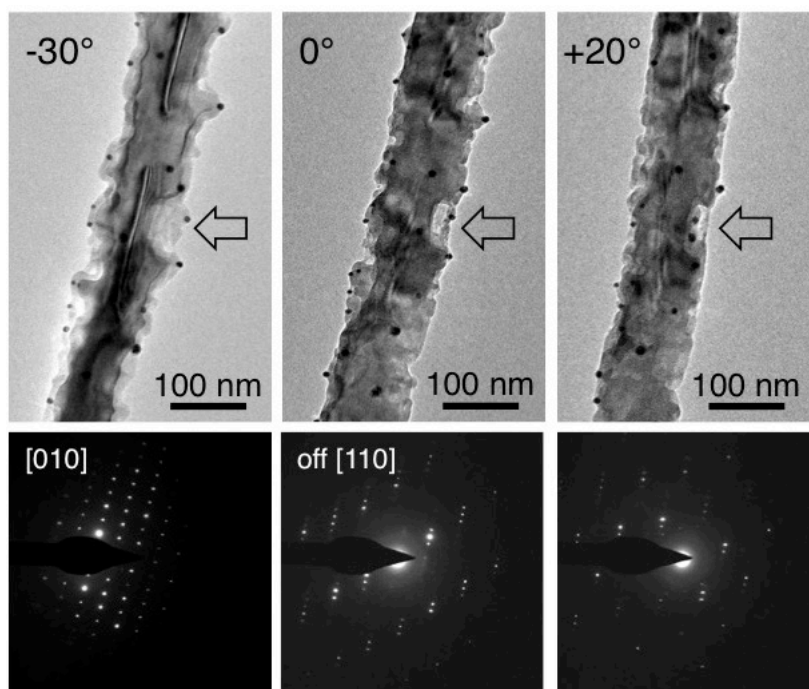
Figure S3. TEM of a partially decomposed GeS nanowire at different tilts. Left: -30° tilt, which is close to the [010] zone axis as shown by the selected-area electron diffraction pattern shown below the real-space image. **Center:** 0° tilt, which brings the wire off the [110] zone axis. **Right:** +20° tilt. Note the different roughness of the nanowire surface and the different appearance of the trench marked by arrows under the different projections.
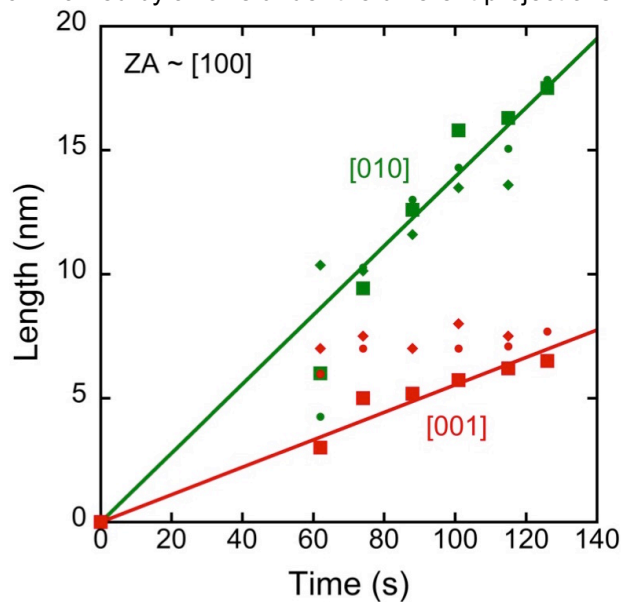
Figure S4. Analysis of the material removal rates within the GeS basal plane and across the van der Waals gaps. Wire shown in Fig. 5 of the manuscript. The rate of GeS removal is ~2.5 times slower along the wire axis (i.e., between layers) than perpendicular to it (i.e., within the layers).
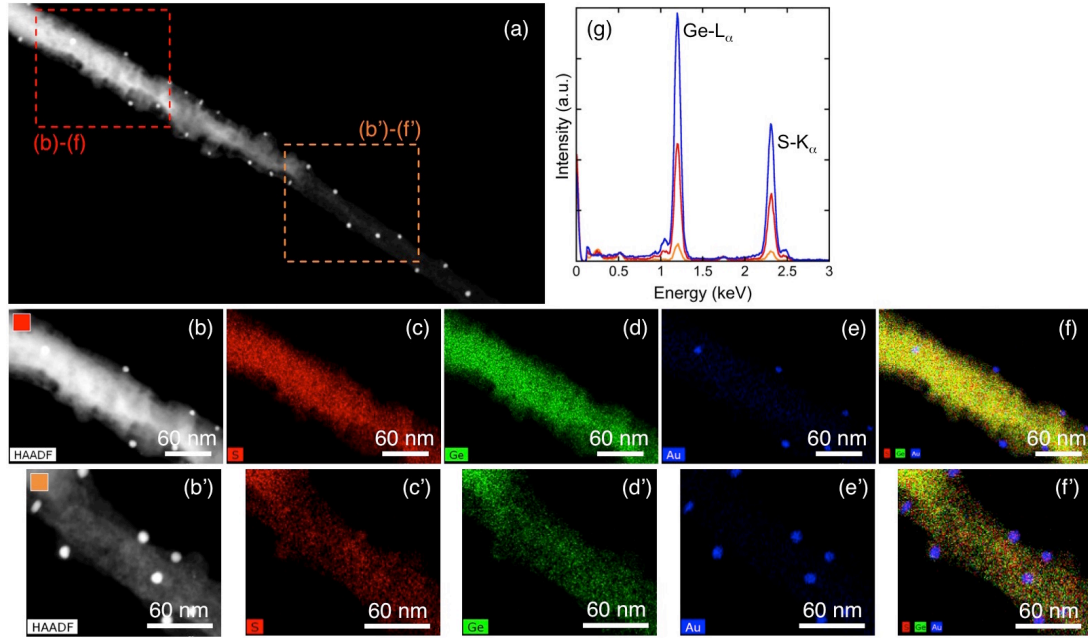
Figure S5. Overview HAADF-STEM image of a representative GeS nanowire after annealing to 260°C. **(a)** HAADF-STEM image showing sections of moderate (red) and advanced decomposition (orange) of the wire. **(b, b')** HAADF-STEM images obtained in the areas marked by rectangles in (a). **(c, c'), (d, d'), (e, e')** EDS chemical maps of the GeS NW showing the distribution of S (red), Ge (green), and Au (blue). **(f, f')** Overlaid S, Ge and Au map from the two parts of the NW. **(g)** EDS spectra from the NW before annealing (blue), and after annealing in the two selected areas (red and orange, respectively).
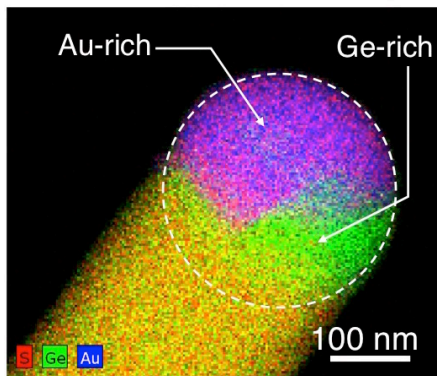
Circle radius r_{tip} = 146 nm
Wire radius r_{wire} ~ 134 nm
~1/3 of the tip is pure Ge
Density ρ_{Ge} = 5.323 g/cm^3
Molar mass μ_{Ge} = 72.63 g/mol
No. of Ge atoms in the tip N_{Ge} = 5.65 x 10^8

Wire length L ~ 20 µm
No. of S atoms released by dissoc. of GeS N_S = 5.65 x 10^8
Density ρ_{GeS2} (Materials Project) = 2.568 g cm^{-3}
Molar mass μ_S = 32.06 g/mol
Volume of GeS$_2$ shell V_{GeS2} = 1.7 x 10^7 nm^3 = 2π r_{wire} d
➔ **Thickness of GeS$_2$ shell: d ~ 1 nm**

Figure S6. Estimate of the thickness of the GeS$_x$ shell (assuming for simplicity a composition ~ GeS$_2$). Left: Composite EDS map of the VLS tip (see also Fig. 3 of the manuscript). Right: Numerical values used in the estimate of the thickness of the S-rich shell around the GeS nanowires.
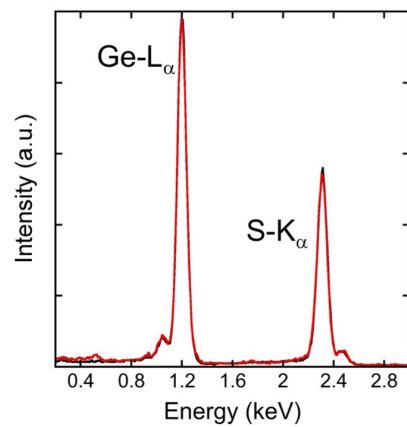
Figure S7. EDS spectra from representative GeS NWs measured immediately after growth and after environmental exposure of the NWs for 95 days (black and red curves, respectively).

2. Supplementary Movies (Thermal decomposition of the GeS nanowires)

Movie M1: GeS nanowire thermal decomposition at 260°C. Zone axis ~ [100]. Times as given in Figure 5 of the manuscript (Total duration of movie: 5 min)
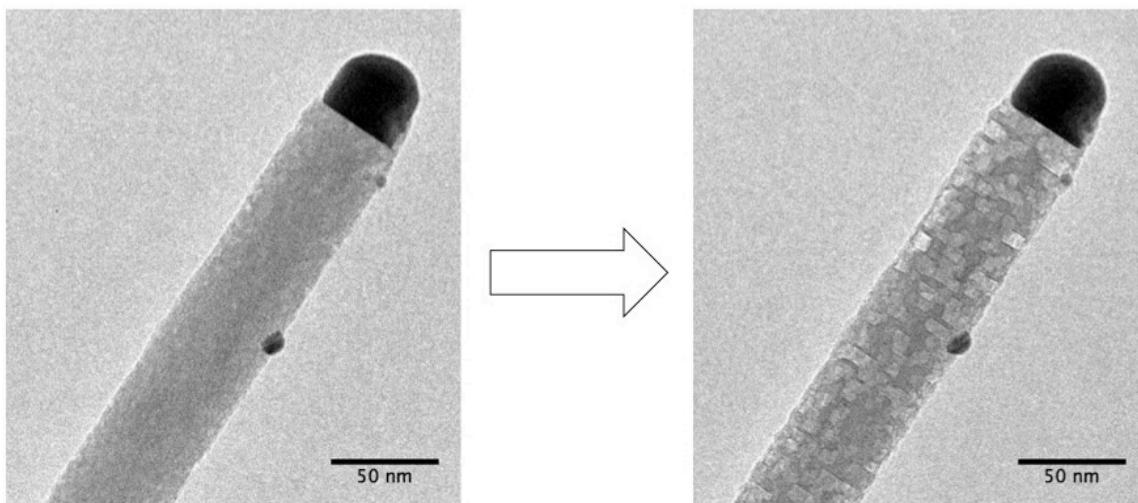
Movie M2: GeS nanowire thermal decomposition at 240°C. (Total duration of movie: 42 min 8 sec)
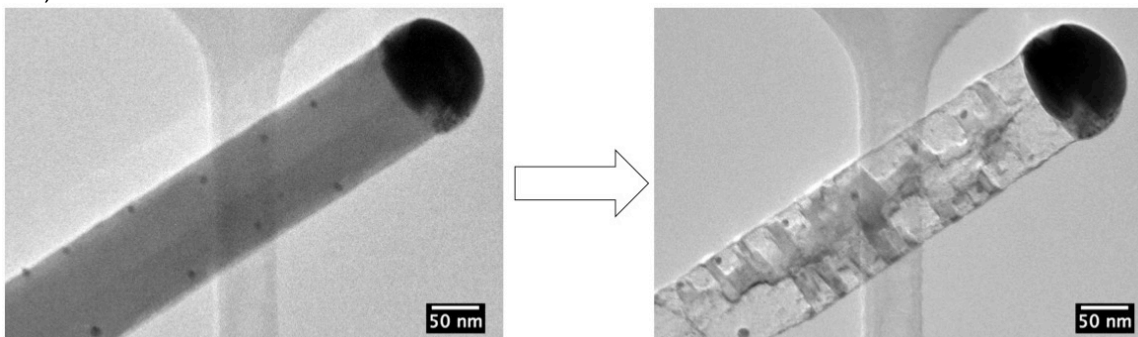
Movie M3: GeS nanowire thermal decomposition at 240°C. Zone axis ~ [010]. Times as shown in the movie (Total duration of movie: 8 min 37 sec)